

Appendix from S. K. J. R. Auld et al., “Predators and Patterns of Within-Host Growth Can Mediate Both Among-Host Competition and Evolution of Transmission Potential of Parasites”

(Am. Nat., vol. 184, no. S1, p. S77)

Experimental and Mathematical Details

This appendix provides additional methods used in the experiments. We also show some more empirical results, including evidence for bacterium-induced gigantism (fig. A1) and a look at the transmission rate of other strains of the bacterium (fig. A2). Then, we more fully explain modeling results presented in figures 3 and 4 in the main text. We also detail calculation of the net reproductive ratio (R_0) for the models using the next-generation matrix approach (fig. A3). Finally, we illustrate an example of coexistence of parasites driven via oscillations (fig. A3B). Those three-species oscillations come from cycles generated by host-bacterial interactions, which we characterized numerically (fig. A4).

Additional Empirical Methods

Within-Host Growth and Transmission Potential

Host and parasites. For all our experiments, we used a clonal genotype of *Daphnia* (H37) that was propagated from a single wild-caught female from Midland Lake, Greene County, Indiana, in 2010. Our isolate of the bacterium (isolate G) was collected from Midland Lake at the same time. This isolate was propagated from a single wild-infected host. It was initially propagated in the laboratory by feeding it to a mixture of *Daphnia* genotypes (H4, H37, and H119, all from Midland Lake) to maximize the likelihood of infection success. After this initial infection cycle, the parasite was propagated using the H37 genotype only and stored at 5°C. The isolate of the fungus arose from multiple infected *Daphnia* collected from Baker Lake, Barry County, Michigan, in 2003 and was propagated on a single host genotype (referred to as the “standard” genotype, also collected in Michigan) until immediately before this study. Then, it was maintained on our experimental *Daphnia* genotype (H37) for two infection passages.

Rearing and experimental conditions. *Daphnia* were maintained individually for three generations prior to experimentation under high food conditions (20,000 *Ankistrodesmus falcatus* algal cells day⁻¹) in 40 mL of medium (50% artificial *Daphnia* medium [Klüttgen et al. 1994] and 50% filtered lake water). Experimental animals consisted of second-clutch neonates (<24 h old) from third-generation maternal lines. These neonates were exposed to one of two parasite treatments: either 2,000 spores mL⁻¹ of bacterial spores or 1,000 spores mL⁻¹ of yeast spores, with levels chosen based on prior and pilot experiments to ensure high prevalence of infection among hosts. Parasite spore solutions were created by gently crushing and diluting previously infected *Daphnia*: 149 *Daphnia* were exposed to the bacterium, and 168 *Daphnia* were exposed to the fungus. After 24 h in the parasite treatment, individual *Daphnia* were changed into fresh medium, kept at 20°C under a 16L : 8D photoperiod, and fed 10,000 *Ankistrodesmus* cells day⁻¹. We moved animals to clean medium (removing offspring) three times per week. Hosts were checked daily for survival, and dead hosts were stored individually at 5°C so that the number of parasite transmission spores per host could be determined. Additionally, live hosts were randomly sampled at fixed times throughout the experiment (see table A1 for details) and stored individually at 5°C. Transmission spore counts were made within 48 h of sampling using a Neubauer (improved) hemocytometer; four independent counts were made from each sample, and the mean was used for further analysis.

Selection on Parasite Within-Host Growth

We evaluated the potential for both spore production and transmission rate to evolve using selection lines that mimicked high- and low-predation environments. High-predation environments were simulated by killing hosts 13 days after parasite exposure, and low-predation environments were simulated by killing hosts 20 days after parasite exposure. We had 8 replicate selection lines for each parasite × predation treatment, for a total of 32 selection lines. A replicate selection line consisted of a beaker containing 150 mL of *Daphnia* medium and 15 *Daphnia* (H37 genotype, 6 days old, established from maternal lines kept under controlled conditions; see above), and was kept under standard food and temperature conditions throughout.

Our goal was to mimic predation by the sloppy predator, *Chaoborus*. The sloppy predator swallows *Daphnia* prey

whole but later regurgitates the carapace and spores that were contained therein. Spores released with the corpses remain highly infective (see Cáceres et al. 2009). We added parasite transmission spores to each beaker (1,000 bacterial spores mL⁻¹ or 500 fungal spores mL⁻¹). *Daphnia* were moved to fresh parasite-free medium 24 h later. High-predation selection lines were kept under standard conditions for 13 days, after which all adult *Daphnia* from each replicate line were placed in a microcentrifuge tube and stored for 8 days at 5°C. Previous work has shown that spores of both of these parasites do not lose infectivity over this time span (A. J. Tessier et al., unpublished data; King et al. 2013). Low-predation selection lines were kept under standard conditions for 20 days, after which the adult *Daphnia* were stored for 1 day at 5°C. For each replicate, *Daphnia* were then gently homogenized and all of the resulting parasite solution was added to a fresh beaker containing 15 healthy *Daphnia* for either 13 or 20 days, as before. This process was repeated five times for the bacterium and six times for the fungus. Some selection lines were lost during the study: after five passages of the bacterium and six passages of the fungus, there were a total of four rapid-growth lines and six slow-growth lines for the bacterium, and five rapid-growth lines and seven slow-growth lines for the fungus.

We examined the effects of simulated predator-mediated selection on the parasites by exposing a single genotype of *Daphnia* (H37) to spores from each of the parasite selection lines. Replicate beakers contained six *Daphnia* in 100 mL of medium and were exposed to parasite spores (1,000 bacterial spores mL⁻¹ or 500 fungal spore mL⁻¹). There were four treatments per parasite: hosts were exposed to parasites from either the high- or low-predation selection lines and were harvested either 13 days (short infection duration, mimicking a high-predation environment) or 20 days (long infection duration, mimicking a low-predation environment) after parasite exposure. On the day of harvest, the proportion of infected hosts per beaker was recorded and the number of spores per host was determined using a Neubauer (improved) hemocytometer (see above).

For each parasite, transmission rate (β) was estimated using the same infection model as in the parameterization study. This produced a single estimate of transmission rate for each replicate selection line. The effect of selection regime (high or low predation) on the transmission rate (β) of each parasite species was analyzed using a Welch's two-sample *t*-test. The number of mature spores per infected host (σ) was also analyzed for each parasite using a linear mixed model. Selection regime (high or low predation) and assay environment (short or long infection duration) and their interaction were fitted as fixed effects; beaker nested within replicate was fitted as a random effect.

Additional Empirical Results

Evidence for Bacterial-Induced Gigantism

Body size data from the within-host growth experiment revealed evidence for bacterial-induced gigantism. The bacterium (*Pasteuria ramosa*) induces gigantism in its host from European ponds, *Daphnia magna* (Ebert et al. 2004). Gigantism is part of the strategy of the life history of some castrators: if parasites can shunt energy allocated to reproduction into growth of the host, then the parasite can benefit (Ebert et al. 2004; Bonds 2006; Hall et al. 2007). These benefits accrue because larger hosts store more parasites and assimilate energy faster (since feeding rate increases with body size), thereby fueling growth of parasites within hosts (Hall et al. 2007). We looked for gigantism by modeling change in size through time using cubic splines (i.e., the smoothing splines algorithm implemented in Matlab R 2011, with smoothing parameter p set close to zero to produce a smooth fit). We added pointwise, 95% confidence intervals using 5,000 bootstraps to these fits. For both parasites, we fit spline-based growth models to infected hosts or to those exposed but not successfully infected (as shown in fig. A1A–A1D). As expected, the fungus showed no evidence for gigantism. Hosts that were infected were of similar size to those that were exposed but not infected (i.e., the 95% confidence envelopes on the spline models overlapped; fig. A1E). In contrast, hosts infected with the bacterium grew larger than those that were exposed but not infected—at least within a window from approximately days 16 through 23 (the 95% confidence envelopes did not overlap during this period). During this window, spore production increased rapidly in infected hosts (see fig. 2E). After day 23, growth through time of infected hosts slowed greatly, becoming similar to that of their uninfected counterparts (fig. A1E). At this point, spore production also plateaued at the maximum level (the carrying capacity; fig. 2E).

Variation in Transmission Rate among Other Bacterial Strains

We estimated transmission rate, β , for several other parasite strains from Midland Lake (Greene County, Indiana). The data were published previously (fig. 1 from Auld et al. 2012); here, we calculated β for each strain, averaged over six clonal genotypes of the host. The estimate used in the modeling figures, from strain G, resembled that from three of the four other strains (as inferred from overlapping confidence intervals). Strain D had lower infectivity (fig. A2).

More Detailed Modeling Results

Invasion Thresholds, Minimal Host Requirements, and Competitive Outcomes

The outcome of competition between parasites in the long run (i.e., at equilibrium) largely depends on two key quantities. To match their depictions in the associated figures, these quantities are expressed in terms of sloppy predation rate (f_C). These quantities are all bounded by an upper predation limit on hosts without disease. This disease-free boundary equilibrium for hosts (S_b^*) is

$$S_b^* = \frac{b - d - f_C - f_F}{bc} = \frac{b - d - f_F}{bc} - \left(\frac{1}{bc}\right)f_C. \quad (\text{A1})$$

Host density decreases linearly with f_C (fig. 3B) until a maximal predation intensity, \hat{f}_C is reached (where $\hat{f}_C = b - d - f_F$). Assuming this condition is met, then parasite j can invade; that is, its reproductive ratio, R_0 , is greater than 1 when

$$R_0 = \frac{S_b^*}{S_j^*} > 1. \quad (\text{A2})$$

This threshold is the ratio of the disease-free boundary equilibrium (eq. [A1]) to the density of susceptible hosts during epidemics (i.e., at the interior equilibrium), S_j^* . When these two densities are equal ($S_b^* = S_j^*$), then $R_0 = 1$ (see below for a formal derivation of R_0 using the next-generation matrix approach). If $S_b^* > S_j^*$, then parasite j can invade and also persist with the host. This threshold can be viewed from a resource competition perspective. If susceptible hosts (S) provide the population-level resource of the parasite, then invasion occurs when the system supplies sufficient resource (S_b^*) to meet the minimal resource requirement of the parasite, itself a consumer (S_j^*). This minimal resource requirement, in turn, is the ratio of losses to gains for both stages of the parasite, I_j and Z_j . For instance, for model 1 (standard obligate killer model, where spore release follows death from infection or nonconsumptive mortality), this minimal host quantity is

$$S_j^* = \frac{m(d + v_j + f_C + \theta f_F)}{(d + v_j)\sigma_j\beta_j}, \quad (\text{A3})$$

where the numerator is the product of losses of Z_j and I_j , respectively while the denominator is the product of gains of these two classes, respectively. In model 1, this S_j^* quantity increases with sloppy predation (i.e., $\partial S_j^*/\partial f_C > 0$; fig. 3B): mortality without spore dispersal increases the minimal host requirement for the parasite. Eventually, with high enough f_C , the system cannot support the parasite as the invasion/feasibility threshold is reached (i.e., when $R_0 = 1$), at

$$f_C = \frac{b\sigma\beta(d + v) - bcm(d + v + \theta f_F) - \sigma\beta(d + v)(d + f_F)}{\sigma\beta(d + v) + bcm}, \quad (\text{A4})$$

where j subscripts were dropped for simplicity. As illustrated in model 1, the bacterium can withstand (slightly) more predation (f_C) than can the fungus (fig. 3B).

Model 2 (simple sloppy predation) considers a scenario where spore release from sloppy predators provides the sole source of spores into the habitat of hosts (the water column). In model 2, predators release a fixed proportion of a maximal spore load ($\lambda\sigma_j$) upon death from predation. With these assumptions, model 2 produces a new minimal resource requirement for parasite j , S_j^* :

$$S_j^* = \frac{m(d + v_j + \theta f_F + f_C)}{\lambda f_C \sigma_j \beta_j}. \quad (\text{A5})$$

This expression has the same numerator (specifically, the product of loss rates of spores multiplied by that of the infected host class) but a different denominator than model 1 (eq. [A3]). The denominator now is the product of gains to spores following sloppy predation ($\lambda f_C \sigma_j$) multiplied by gains to the infected host class (β_j). With this change, the minimal host requirement now decreases along a gradient of the rate of sloppy predation (f_C ; $\partial S_j^*/\partial f_C < 0$ always; fig. 3B). Thus, two invasion thresholds now emerge at $\hat{f}_{C,i}$:

$$\hat{f}_{C,i} = \frac{X - Y}{2} \pm \sqrt{\frac{(X - Y)^2}{4} - Y(d + v + \theta f_F)}, \quad (\text{A6})$$

where

$$X = b - d - f_F, \quad (\text{A7a})$$

$$Y = \frac{bcm}{\lambda\sigma_j\beta_j}. \quad (\text{A7b})$$

The lower and upper f_C threshold appears (fig. 3B) for each parasite; this feature of model 2 reappears in model 3. These thresholds also mean that parasite invasion (i.e., $R_0 > 1$) requires enough but not too much sloppy predation. More specifically, the upper threshold reflects the negative effects of mortality inflicted by the sloppy predator (as in model 1, too). But now, the lower threshold captures the positive effects of spore spreading by sloppy predators. A certain intensity of sloppy predation is needed to initiate an epidemic. Thus, over some range of f_C , R_0 increases (fig. A3A), where R_0 (calculating using the next-generation approach again, illustrated below) is

$$R_0 = \frac{\lambda f_C \sigma_j \beta_j S_b^*}{m(d + v_j + \theta f_F + f_C)}. \quad (\text{A8})$$

Higher fish predation (f_F) pushes the R_0 curves down along the f_C axis (fig. A3A).

Assuming both parasites can invade, competitive outcomes depend on minimal resource requirements. Better competitors have a lower ratio of losses (numerator) to gains (denominator; eqq. [A3], [A5]). Thus, they can depress density of susceptible hosts to lower levels than needed by their competitors (i.e., better competitors have lower S_j^*). For model 1, the bacterium is the superior competitor (fig. 3A). The bacterium wins, assuming equivalent loss rate of spores from the environment (m), because it has higher transmission potential (spore yield \times transmission rate, $\sigma_j\beta_j$) when hosts die from infection (see fig. 2F; $\partial S_j^*/\partial(\sigma_j\beta_j) < 0$). This superiority occurs even though the bacterium exerts lower virulence on survivorship, a feature that undermines its competitive advantage (i.e., the bacterium has lower v_j , which raises S_j^* , since $\partial S_j^*/\partial v_j < 0$).

Model 3 (sloppy predation and within-host growth model) incorporates the timing of within-host growth. Some results for this model mirror those of model 2, but some new ones emerge. (Note, however, that it becomes very difficult to derive analytical expressions for some of the thresholds involved.) First, two thresholds of predation intensity arise (as seen in model 2). They stem from two intersections of the disease-free equilibrium (S_b^*) with the minimal host requirement (S_j^*); S_j^* can now decrease over some range of f_C due to the benefits of spore dispersal from sloppy predators (fig. 3C). Thus, the new lower threshold of predation encapsulates those benefits. This lower threshold means epidemics require some sufficient level of sloppy predation to initiate. However, in model 2, S_j^* only decreases with f_C . In model 3, S_j^* begins to increase again with f_C because intense predation means per host spore production declines—infected hosts die carrying fewer spores when f_C is high. Second, the ranking of upper predation thresholds can change between parasites. Along an increasing gradient of f_C , predation removes the bacterium from the system before the fungus (fig. 3C). This result stems from differential within-host growth of hosts between parasites (best seen in fig. 2G). At higher predation intensity (i.e., less time to grow within the host, on average, for the parasite), the fungus has greater transmission potential than the bacterium, due to the greater transmission rate of the spores produced. (Consequently, S_j^* increases less steeply with f_C for the fungus than for the bacterium.) Third, the different schedules of within-host growth can reverse competitive superiority of the bacterium. At a certain intensity of sloppy predation, the fungus becomes the competitive dominant (because it now has a lower S_j^*). Thus, the combination of sloppy predation and within-host growth can reverse competitive superiority of the parasites.

These thresholds govern outcomes of competition among parasites along gradients of predation or epidemiological trait space. Given the estimated parameters, model 1 (standard obligate killer model) and model 2 (simple sloppy predation model) predict that the bacterium should retain competitive superiority over the fungus along very broad gradients of intensity of fish predation (f_F) and sloppy predation (f_C ; fig. 4A, 4B). The shape of the invasion thresholds differ for each model in f_F - f_C space. In model 1, these relationships decrease because both predators essentially act identically—they just impose mortality on the host and parasite. These thresholds become hump-shaped for model 2 because sloppy predation releases spores. Thus, the parasite can withstand little fish predation when f_C is low (i.e., when few spores are released). As f_C increases, the parasite can withstand much more fish predation as sloppy predation fuels disease spread. But, as f_C increases further still, the negative effects of sloppy predation begin to dominate, and the invasion curve bends back down. Nonetheless, in both cases, when they could persist together, the bacterium has the lower S_j^* (as parameterized). Thus, it remains competitively dominant. Note also that, in both cases, there is little parasite-free parameter space for hosts—both parasites are good at invading and persisting as long as hosts are present.

The combination of within-host growth of the parasite and sloppy predation in model 3 changes these outcomes, however. First, predation now limits both parasites to less parameter space (i.e., the no-parasite region occupies much more f_C - f_F space in fig. 4C than in fig. 4A, 4B). More interestingly, model 3 predicts shifts in competitive dominance

among parasites in f_C - f_F space. The bacterium still dominates environments with less sloppy predation (i.e., at lower f_C , where it still can produce many more fungal spores within hosts). However, with sufficiently high f_C , the fungus enjoys a competitive advantage (due to faster within-host growth) and can outcompete the bacterium (i.e., it can have a lower S_j^* ; see also fig. 3C). The fungus now can also withstand higher intensity of sloppy predation (i.e., the fungus-only region of fig. 4C). The small region of coexistence stems from bacterium-driven oscillations (and thus provides an example of coexistence through Chesson’s [2000] concept of “relative nonlinearities”; fig. A3B). However, this region is relatively small compared to the others (fig. 4C–4E). Not surprisingly, at a given level of fish predation (f_F), the fungus becomes increasingly dominant when hosts better resist infection from the bacterium (lower β_B ; fig. 4D) or when infected hosts produce lower maximal density of spores (lower σ_B ; fig. 4E). But most importantly, these three examples (fig. 4C–4E) show how key facets of natural history in this system—within-host growth schedules, sloppy predation, and the environmental trap—creates a niche for the fungus to dominate competition over the bacterium. In essence, the fast schedule of the fungus can upend the competitive superiority of the bacterium, given sufficient intensity of sloppy predation.

R₀ of the Core Model Using the Next-Generation Approach

In the text, we state that the net reproductive ratio, R_0 , for each model is the ratio of the density of susceptible hosts in disease-free systems (i.e., at the boundary equilibrium, S_b^*) divided by the minimal host requirement for epidemics (i.e., the density of susceptible hosts at the interior equilibrium, S_j^*). In support, here we derive R_0 for model 1 as an example. We will follow the approach using the next-generation matrix (\mathbf{G}) approach (Diekmann and Heesterbeek 2000). This method requires determining a matrix \mathbf{F} that accounts for “new” infections (“transmission”) and matrix \mathbf{V} , which accounts for transfer of parasite (“transition”) between its two compartments, infected hosts (I) and environmentally distributed spores (Z). Transmission matrix \mathbf{F} is

$$\mathbf{F} = \begin{bmatrix} 0 & \beta_j S_b^* \\ 0 & 0 \end{bmatrix}, \quad (\text{A9})$$

that is, new infections only come from contact of spores with susceptible hosts (at their disease-free equilibrium). The transition matrix \mathbf{V} is

$$\mathbf{V} = \begin{bmatrix} -(d + v_j + \theta f_F + f_C) & 0 \\ \sigma_j(d + v_j) & -m \end{bmatrix}. \quad (\text{A10})$$

Using this methodology, R_0 is then the dominant eigenvalue (spectral radius) of $\mathbf{G} = -\mathbf{FV}^{-1}$, which is

$$R_0 = \frac{\sigma_j(d + v_j)\beta_j S_b^*}{m(d + v_j + \theta f_F + f_C)} = \frac{S_b^*}{S_j^*}. \quad (\text{A11})$$

Thus, R_0 is the ratio of the boundary equilibrium, S_b^* —the host density provided by the system without infection—to the minimal resource requirement of the parasite, S_j^* . R_0 exceeds 1, permitting invasion of the parasite, when the system provides hosts at a density that exceeds its minimal host (resource) requirement.

Host-Bacterium Oscillations

Given the parameter values used, the bacterium (but not the fungus) can generate host-parasite oscillations. Oscillatory versus stable regions are shown on figure 4, but we had to use numerical methods to delineate them. We used a root finder (FindRoot in Mathematica 8.0) to trace out the three Routh-Hurwitz (RH) criteria. Those RH criteria depend on elements of the Jacobian matrix of the three-dimensional ordinary differential equation system (i.e., the subsystem for only the bacterium, without the fungus). Each of the three model variations had the same basic Jacobian structure,

$$\mathbf{J} = \begin{bmatrix} J_{11} & J_{12} & J_{13} \\ J_{21} & J_{22} & J_{23} \\ 0 & J_{32} & J_{33} \end{bmatrix}. \quad (\text{A12})$$

A matrix such as \mathbf{J} has three coefficients of its characteristic polynomial, $\lambda^3 + A_1 \lambda^2 + A_2 \lambda + A_3$, where

$$A_1 = -(J_{11} + J_{22} + J_{33}), \quad (\text{A13a})$$

$$A_2 = -(J_{12}J_{21} - J_{11}J_{22} + J_{33}J_{32} - J_{11}J_{33} - J_{22}J_{33}), \quad (\text{A13b})$$

$$A_3 = -(J_{13}J_{21}J_{32} - J_{11}J_{23}J_{32} - J_{12}J_{21}J_{33} + J_{11}J_{22}J_{33}). \quad (\text{A13c})$$

Stability requires that $A_1 > 0$, $A_3 > 0$, and $A_1 A_2 - A_3 > 0$. The second condition typically denotes the invasion ($R_0 = 1$) threshold, but the third condition separates stable from unstable (oscillatory) dynamics.

The three models have a similar Jacobian matrix, except for J_{32} :

$$\mathbf{J} = \begin{bmatrix} b[1 - c(I + 2S)] - b_I c S^* - d - \beta Z^* & b_I [1 - c(2I + S)] - bc S^* & -\beta S^* \\ \beta Z^* & -(d + \nu + \theta f_F + f_C) & \beta S^* \\ 0 & J_{32} & -m \end{bmatrix}, \quad (\text{A14})$$

where we have dropped subscripts for simplicity (above and below), and values of J_{32} can be

$$\text{Model 1: } (d + \nu)\sigma, \quad (\text{A15a})$$

$$\text{Model 2: } \lambda f_C \sigma, \quad (\text{A15b})$$

$$\text{Model 3: } \lambda f_C \sigma (f_C). \quad (\text{A15c})$$

Elements of these Jacobian matrices were evaluated at the interior equilibrium ($S^* > 0$, $I^* > 0$, $Z^* > 0$) to calculate the coefficients of the characteristic polynomial (eq. [A9]).

Based on parameter values used in this study, the bacterium but not the fungus has the propensity to trigger oscillations with its host. Keeping mortality from predation (f_F, f_C) constant, we can see that key traits of the fungus create the instabilities: high maximal production of spores (σ), minimal virulent effects on survival (ν), quite strong virulent effects on fecundity of hosts (b_I), and sufficiently high transmission rate (fig. A4). Based on the bifurcation diagrams, the generation of oscillations hinges especially on the combination of strong depression of host fecundity ($b_I = 0.05 \text{ day}^{-1}$ in our figure) and high parasite production ($\sigma = 23.6 \times 10^5$ spores/host).

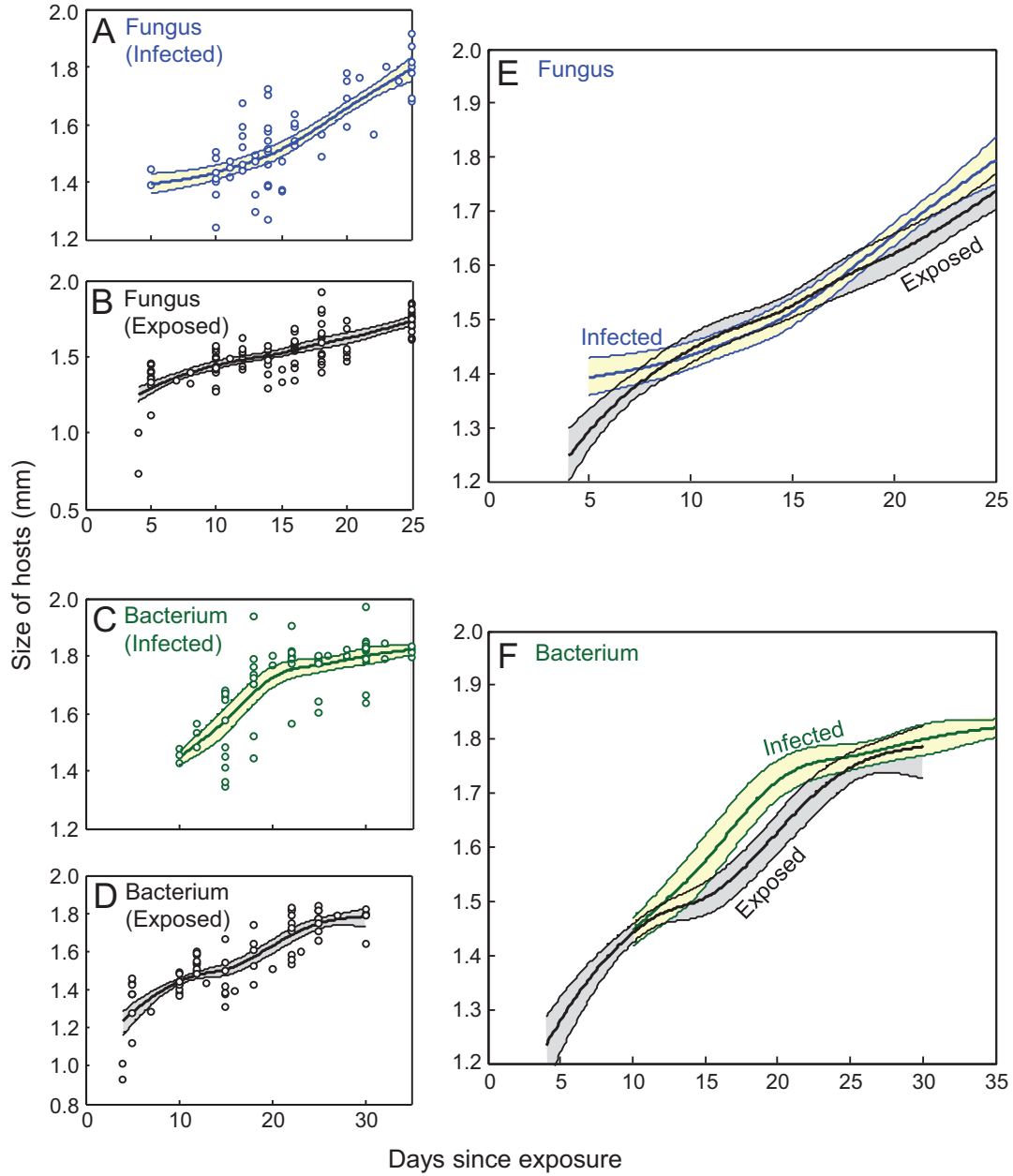


Figure A1: Evidence for bacterial-induced gigantism in the within-host growth experiments. *A–D* show cubic spline models, with 95% confidence envelopes, fit through size data following exposure to either the fungus (*A, B*) or the bacterium (*C, D*). All hosts were exposed to parasites, but some become infected (*A, C*), while others remained uninfected (*B, D*). Based on these spline models of size through time, the fungus (*E*) showed no evidence for gigantism, as expected (i.e., the confidence envelopes overlapped), but the bacterium (*F*) did during a window of about days 16–23.

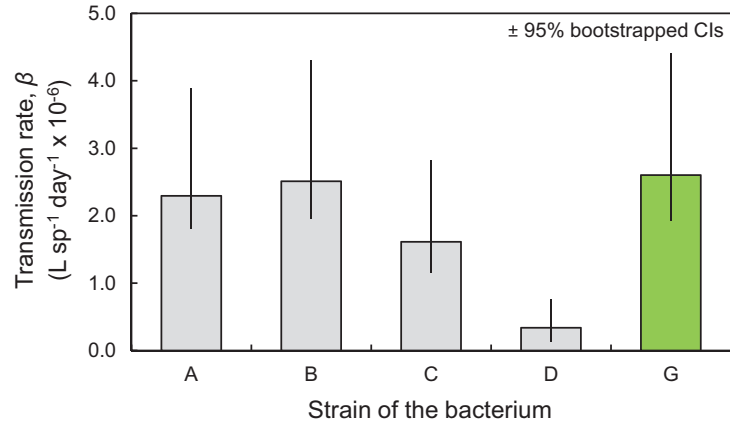


Figure A2: Transmission rate of five different strains of the bacterium (*Pasteuria ramosa*). Each bar is the mean of estimates from six different genotypes of the zooplankton host (*Daphnia dentifera*). Data were previously published elsewhere (Auld et al. 2012). Data from strain G (in green) was used to parameterize the model.

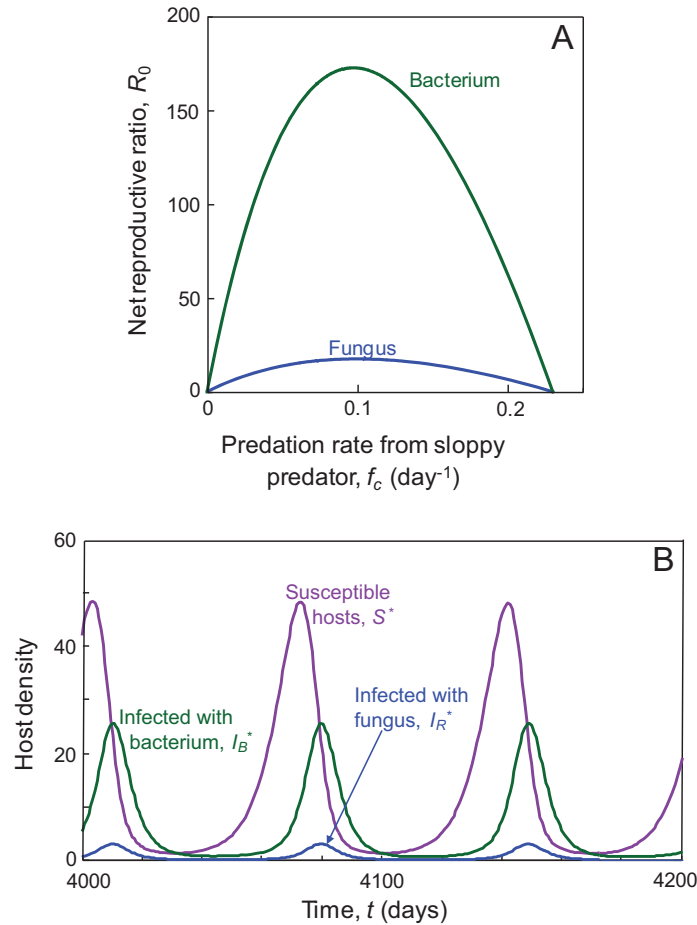


Figure A3: Additional modeling results. *A*, Model 2: when sloppy predators alone release spores from infected hosts, R_0 becomes a unimodal (hump-shaped) relationship, with invasion thresholds (i.e., $R_0 = 1$) at both low and high intensities of sloppy predation (f_c). *B*, Model 3: an example of the two parasites coexisting through cycles generated by the bacterium ($f_B = 0.05, f_C = 0.0595$). This interesting type of behavior is possible but occupies little of parameter space in the bifurcation diagram (fig. 4C).

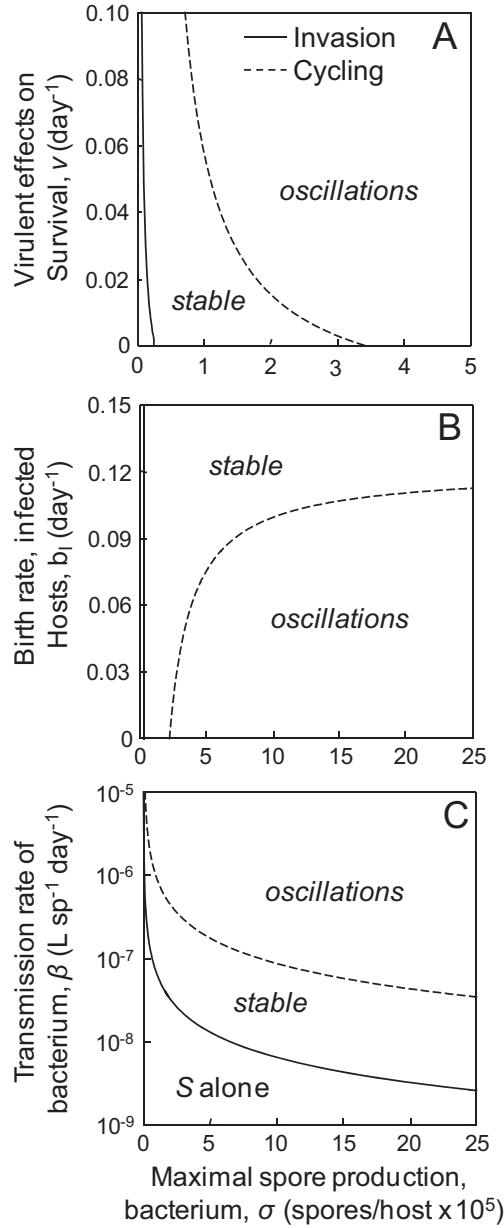


Figure A4: Epidemiological drivers of cycling of the host-bacterium system alone, illustrated for model 1 (a traditional *SIZ* model for an obligate killer). For all bifurcation diagrams, two thresholds denote when the parasite can invade (i.e., $R_0 = 1$, solid line) and the origin of oscillations (when the third Routh-Hurwitz condition is not met [see text]; dashed line). These two thresholds create three dynamical possibilities: susceptible hosts persist alone, stable host-parasite dynamics, and host-parasite cycles. Along an increasing gradient of maximal spore production, oscillations are more likely at higher infection-enhanced mortality rate on hosts, v (A), lower birthrate of infected hosts, b_i (B), and higher transmission rate, β (C). In these examples, mortality from predation from fish (f_F) and the sloppy predator *Chaoborus* (f_C) are held constant ($f_F = 0.05$, $f_C = 0.05$). (For the parameters used, the host-fungus system yields only stable dynamics [assuming $R_0 > 1$].)

Table A1. Sampling regime for hosts exposed to the bacterium and the fungus

Day of death	Number of harvested hosts	
	Exposed to bacterium	Exposed to fungus
5	8	15
10	13	15
12	13	15
14	...	15
15	18	...
16	...	15
18	18	15
20	...	9
22	18	...
25	18	18
30	18	...
35	4	...

Note: Dates of harvest were chosen based on preliminary experiments, which showed that the fungus killed hosts sooner than the bacterium.

Table A2. Analysis of the spore yield (σ) of two parasites

	Spore yield (σ)	
	Test statistic	<i>P</i>
Fungus:		
Fixed effects:		
Selection treatment	$F_{1,10} = 1.46$.25
Assay environment	$F_{1,35} = 42.55$	<.0001
Selection \times assay	$F_{1,35} = .43$.52
Random effect:		
Beaker (replicate)	$\chi^2_1 = 2.88 \times 10^{-8}$.99
Bacterium:		
Fixed effects:		
Selection treatment	$F_{1,8} = .004$.95
Assay environment	$F_{1,23} = 31.41$	<.0001
Selection \times assay	$F_{1,23} = 19.91$	<.001
Random effect:		
Beaker (replicate)	$\chi^2_1 = .45$.50

Note: Selection treatment = high- or low-predation selection treatment. Assay environment = length of time infection allowed to develop (short vs. long) during experimental assay; short infection duration mimics a high-predation environment.

Literature Cited Only in the Appendix

- Chesson, P. 2000. General theory of competitive coexistence in spatially-varying environments. *Theoretical Population Biology* 58:211–237.
- Diekmann, O., and J. A. P. Heesterbeek. 2000. *Mathematical epidemiology of infectious diseases*. Wiley, Chichester, UK.
- King, K. C., S. K. J. R. Auld, P. J. Wilson, J. James, and T. J. Little. 2013. The bacterial parasite *Pasteuria ramosa* is not killed if it fails to infect: implications for coevolution. *Ecology and Evolution* 3:197–203.
- Klüttgen, B. U., U. Dülmer, M. Engels, and H. T. Ratte. 1994. ADaM, an artificial freshwater for the culture of zooplankton. *Water Research* 28:743–746.